Time-Minimal Aircraft Trajectory in the Presence of Unsteady Wind by Shape Optimization

James M. Shihua, Chris HC. Nguyen, and Rhea P. Liem
Department of Mechanical and Aerospace Engineering
The Hong Kong University of Science and Technology
Clear Water Bay, Kowloon, Hong Kong SAR.

***Abstract*—Consideration of wind effect in airline operations has become crucial for saving travel time, maximizing operational efficiency, and reducing fuel consumption. In this paper, we propose a new approach to solve the time-minimal trajectory problem by formulating it as a shape optimization problem, accounting for unsteady wind conditions. Unlike traditional methods, our approach works on parameterized trajectory in a continuous spatio-temporal domain, which does not require a discretization in the two-dimensional domain. Furthermore, the approach also simplifies the cost function evaluation, with only one co-dimension along the trajectory. Hence, our approach guarantees continuity of flight states, and is independent of network (also referred to as a mesh or a grid in the literature) quality and constraints. Through a suite of simulations and case studies, we demonstrate the effectiveness of our approach in reducing travel time for various flight types, including long-haul, medium-haul, and short-haul flights. The obtained optimized trajectory is shown to achieve a balance between headwind avoidance and distance minimization, leading to a time-minimal solution. A statistical analysis is performed on three popular flight sectors, HKG-LHR, HKG-ICN, and HKG-TPE, to validate the effectiveness of the developed algorithm in reducing flight time, using flight information extracted from real airline operations. Optimized trajectories are then compared with those from Quick Access Recorder (QAR) data shared by Cathay Pacific Airways. Our findings offer practical implications for airlines seeking to enhance operational efficiency and reduce environmental impact.**

***Keywords*—Trajectory optimization, airline operation, unsteady wind, shape optimization.**

I. Introduction

In an era of increasing air travel demand and growing environmental concerns, striving towards more efficient operations has emerged as a crucial aspect in the aviation industry. Efficiency in aviation operations encompasses various dimensions, including fuel economy, operational efficiency, resource management, to name a few. Fuel efficiency is a key area of focus, as it directly impacts both economic and environmental aspects of air transportation. The International Air Transport Association (IATA) reports that fuel costs account for a substantial portion of airlines' operating expenses, and improving fuel efficiency can notably reduce operating costs [1]. In addition, improving fuel efficiency contributes to the reduction of greenhouse gas emissions, thus mitigating the environmental impact of air travel [2]. In order to reduce fuel consumption and maximize operational productivity for a route, airlines nowadays are paying attention to wind field to take advantage of tailwinds when planing flight trajectories [3]. When cruising with tailwinds, ground speed increases, reducing travel time and fuel consumption.

Trajectory optimization in the presence of wind or current is a long-standing problem in the fields of aviation [4], underwater robotics [5], ship navigation [6], etc. Generally speaking, the problem can be categorized into two, namely (spatially) varying wind and unsteady wind. The same applies to ocean current, but the scope of this work is limited to aircraft and wind. Variable wind means that there exists *only* a spatial variation of wind direction and magnitude, but is constant in time. Unsteady wind, on the other hand, has both spatial and temporal variation. In this paper, we are particularly interested in the latter, especially when long-haul flights are considered, where the variation of wind duration over the flight duration is non-negligible.

Two families of algorithms can be applied to solve the wind-optimal trajectory problem, namely grid-based or grid-free. Grid based algorithms, such as Dijkstra [7] algorithm, A* algorithm [8], D* algorithm [9], etc., discretize the two-dimensional (2-D) spatial domain into a network, or grid, and try to find the nodes (or waypoints) that constitute an optimal path. Dijkstra algorithm is also extended to 3-D by Wang *et al.* [10] to solve unsteady wind problems. This family of algorithms efficiently traverses all nodes in the network and ensures global optimality and completeness [8], and is popular among path-finding problems with complex obstacles. The main drawback of this type of algorithms is that the solution is network-dependent, in that the solution can exist only in the configuration space permissible by the network. In addition, the practicality of the solution depends greatly on the network generation procedure, quality, and spatial resolution, especially for commercial aircraft or ships that are not agile nor easy to maneuver. Last but not least, as the whole 2-D domain needs to be discretized, the algorithm becomes both time- and memory-consuming when the spatial resolution is high.

The above-mentioned algorithms have a competitive edge especially for problems where the nodes and edges must be clearly defined, such as ground transportation. However, for airlines operations, an aircraft does not necessarily always

SESAR Innovation Days
27-30 November 2023
Seville

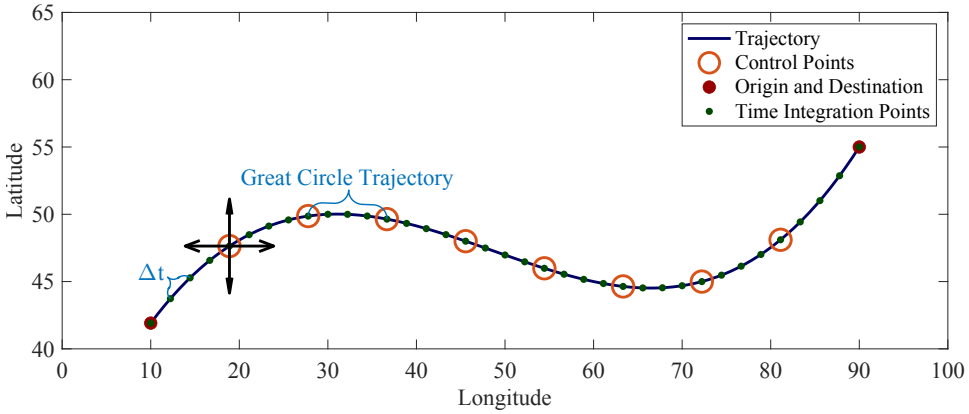

Figure 1. Formulation of the wind-optimal trajectory as a shape optimization problem.

follow links between nodes, especially during the cruising stage. In this situation, algorithms that work in a continuous space are preferred. The traditional approach is to find the best function to represent the shape of the trajectory. Very often, the trajectory optimization problem is converted to a partial differential equation (PDE), called the Eikonal equation

$$||\nabla u|| = \tau, \tag{1}$$

where u is the distance function and τ is the cost function [11]. Such algorithms include the level set method [12], the fast marching method [5], the ordered upwind method [13], etc. However, solving a PDE is still computationally costly, and typically requires 2-D discretization of the whole spatial domain. In addition, this equation is steady-state (no temporal marching term $\frac{\mathrm{d}u}{\mathrm{d}t}$), hence it is not suitable for resolving the optimal trajectory in the presence of unsteady wind.

In this research, we develop a travel-time minimization procedure that can consider the effect of unsteady wind. We assume that the fuel consumption is proportional to the travel time, hence minimizing either quantity will yield the same result. By representing the trajectory as a continuous shape, the method is grid-free and suitable for continuous spatio-temporal domain. The cost-function evaluation (i.e., travel-time calculation) only necessitates the discretization along the continuous trajectory; hence, the problem's co-dimension is one. Such discretization (complexity of $\mathcal{O}(n)$) is much more efficient than the two families of algorithms mentioned above (complexity of $\mathcal{O}(n^2)$). The trajectory is controlled by several design points, which are allowed to move continuously in the 2-D domain. The grid-free property of this approach allows for more flexibility in path planning, which is suitable for aircraft flight operations.

This paper is structured as follows. In Section II, we provide details on the formulation of the trajectory optimization problem, algorithms for trajectory deformation, and computation of the cost function, followed by a brief description of the optimization algorithm. In Section III, we demonstrate the effectiveness of such algorithm by comparing the travel time between optimal trajectory, great circle trajectory, and real operational data obtained from our airline partner, Cathay Pacific Airways Limited (CX). Finally, Section IV summarizes what we have achieved in this research.

II. Methodology

A. Wind-Optimal Trajectory as a Shape Optimization Problem

In this section, we describe the methodology used to optimize the aircraft cruising trajectory in the presence of unsteady wind. This methodology is inspired by airfoil shape design optimization in the context of aircraft design, which is another important branch of aerospace engineering. In airfoil shape optimization, the shape of an airfoil (i.e, the cross section of an aircraft wing) is optimized to achieve a desired performance, which is generally related to its aerodynamic efficiency. To optimize a shape, a parametrization technique must be used to deform or generate a shape. In this research, we adopt the shape parameterization approach by means of deformation [14], where the baseline design is continuously deformed into a new shape as the optimization progresses. Some popular methods belonging to this category include Hicks-Henne function [15], free-form deformation (FFD) [16], *etc*. The new method developed in this work belongs to the FFD category, and its details are presented as follows.

The trajectory $\mathbf{T} = [x(s), y(s), t(s)]^\top$, or its curve shape $[x(s), y(s)]^\top$ (i.e., the shape of the solid black curve in Fig. 1), is controlled by several design points $P_i = (x_i, y_i)$, called control points (a vector of all design points is denoted as $\mathbf{P}$ accordingly). Here, x is longitude, y is latitude, t is time, $i = 1, 2, 3, \ldots, n$ is the index of control points, s is an arbitrary parametrization, and n is the number of control points. It is worth mentioning that, there is no time information in a shape; however, time is implied by the shape and aircraft dynamics. To create a shape from several control points, an interpolation technique is necessary, such as polynomial interpolation, Bezier curve, B-spline, and etc. As a time minimization problem, a great circle (GC) trajectory is filled between two control points, which is the shortest path between two points on the earth sphere. By adding a displacement to a control point (changing its (x, y) coordinate), the trajectory shape can be modified. This type of operation is usually referred to as a free-form deformation (FFD) [17]. With its

shape defined, it is possible to determine the travel time required to follow this path: the trajectory will be further discretized into $N \gg n$ finer segments to perform a time integration. However, the travel time Δt_i between two points (x_i, y_i) and (x_{i+1}, y_{i+1}), in the presence of unsteady wind, is unknown. This is because the arrival time at (x_i, y_i) is unknown and depends on all previous travel time Δt_j where $j \leq i-1$. Hence, Δt_i has to be solved by a sequential or an iterative process in a vectorized manner. For a large N, iterative process has a clear performance advantage over the sequential one, which is adopted in this work and will be explained in Section II-C. Fig. 1 depicts the concept mentioned above: the trajectory (solid dark blue line) from origin to destination (red dots) is generated by control points (solid orange circle) with a GC trajectory filled in between. Time integration points (green dots) are used to calculate the travel time fragments, and their summation is the total travel time.

Having explained the formulation of the optimization problem, here we present the optimization statement:

$$\begin{aligned} \underset{\mathbf{x},\mathbf{y}}{\text{minimize}} \quad & t_f = f\{\mathbf{T}[\mathbf{P}(\mathbf{x},\mathbf{y})]\} \\ \text{subject to} \quad & x_i^{\text{l}} \leq x_i \leq x_i^{\text{u}}, \quad i = 1, 2, \ldots, n \\ & y_i^{\text{l}} \leq y_i \leq y_i^{\text{u}}, \quad i = 1, 2, \ldots, n, \end{aligned} \tag{2}$$

where t_f is the total travel time as a function of trajectory $\mathbf{T}$, thus control points $\mathbf{P}$. x_i^{l}, x_i^{u} and y_i^{l}, y_i^{u} are the lower and upper bound of x_i and y_i, respectively. The problem is formulated to explore the potential time saving by optimizing the flight trajectory without the constraints of waypoints, which exist in reality. Furthermore, no-fly zone and air traffic volume (congestion) along the path are not taken into consideration at this stage of research.

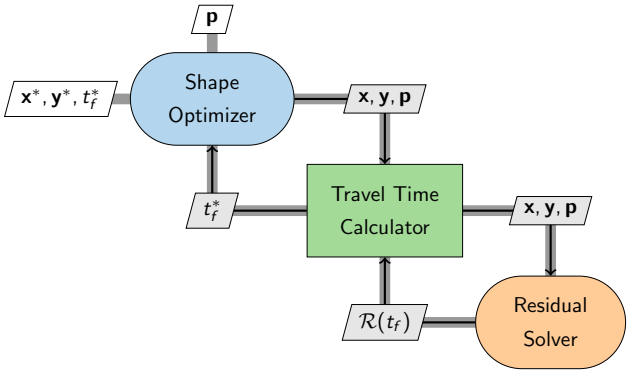

Figure 2. XDSM of the the optimization process.

Fig. 2 illustrates the optimization process using an extended design structure matrix (XDSM) diagram[1]. In this figure, thin black lines with arrows and bold gray lines represent the process flow of the optimization loop and data flow, respectively. A more detailed documentation can be found in its repository. Following the diagram, the shape optimizer iteratively deforms the shape of the trajectory, and evaluate the cost function (t_f) and its gradient. Inside the function call, t_f is calculated by solving the residual equation, which will be further explained in Section II-C.

B. Wind Data Processing and Interpolation

Though this research proposes a grid-free trajectory optimization method, wind data from available resources still come in a grid format (matrix). In our study, we use the ERA5 dataset from European Centre for Medium-Range Weather Forecasts (ECMWF) [2]. These wind data have a resolution of $0.25°$ in latitude, $0.25°$ in longitude, and $1\,\text{h}$ in time, with coverage of the entire globe every day. Hence, for every calendar day, the wind data matrix W_x and W_y has a dimension of $N_x \times N_y \times N_z = 1{,}440 \times 721 \times 24$, where W_x is the east wind and W_y is the north wind. 3-D interpolation using the gridded data is performed to calculate the wind information on each spatio-temporal state $\mathbf{u} = (x, y, t)^\top$. For most robust and efficient implementation, trilinear interpolation is used, which linearly interpolates the value between nodes on a 3-dimensional regular grid. The output of such an interpolation is C_0 continuous, but is once-differentiable everywhere except on the edge and node of the gridded data. Fig. 3 illustrates the continuity and differentiability of a trilinear interpolation. The differentiability of wind data facilitates gradient descent (GD) in the optimizer. The concept is that, the total derivative of the cost function (t_f) with respect to design variables ($\mathbf{x}$ and $\mathbf{y}$) can be computed by the chain rule, which requires all intermediate functions to be at least once differentiable. More details about the optimization subroutine will be explained further in Section II-D.

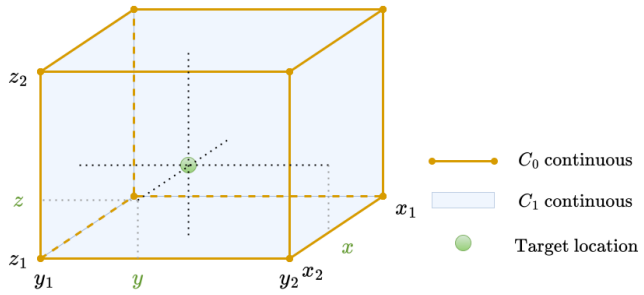

Figure 3. Trilinear interpolation.

C. Travel Time Calculation

To initiate the computation, the algorithm (as illustrated in Algorithm 1) first generates the trajectory using n design points $(\mathbf{x}, \mathbf{y})$. A great circle segment is used to connect two adjacent design points, enriched with N additional time integration points per segment as shown in Fig. 1. The great

[1] https://github.com/mdolab/pyXDSM (last accessed on 13 September 2023)

[2] https://cds.climate.copernicus.eu/cdsapp#!/dataset/reanalysis-era5-pressure-levels?tab=overvie (last accessed on 13 September 2023)

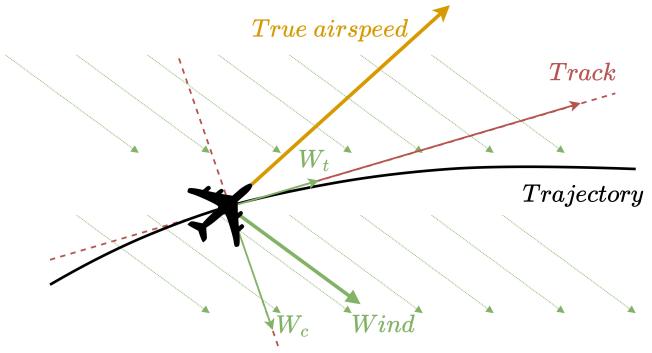

Figure 4. Superposition of wind velocity and true airspeed.

circle distance between two adjacent waypoints (x_k, y_k) and (x_{k+1}, y_{k+1}) can be calculated by

$$\begin{aligned} \mathrm{d}x_k = R\cos^{-1}\left(\cos y_k \cos y_{k+1} \cos\left(x_k - x_{k+1}\right)\right. \\ \left. + \sin y_k \sin y_{k+1}\right), \end{aligned} \tag{3}$$

where $R = 6{,}371$ km is the Earth radius and $k \in [1, N-1]$. Afterwards, the algorithm derives an initial estimation of the travel time between waypoints, denoted as $\mathrm{d}\mathbf{t}$, by

$$\mathrm{d}\mathbf{t} = \frac{\mathrm{d}\mathbf{x}}{\sqrt{V_{\mathrm{TAS}}^2 - W_c^2} + W_t}. \tag{4}$$

where $\mathbf{W}_t$ is the track wind (tangential to T) and $\mathbf{W}_c$ is the cross wind (normal to T). Because $\mathbf{W}_t$ and $\mathbf{W}_c$ are not yet known, they are initialized to $\mathbf{0}$ as an initial guess. The time stamp at each waypoint $\mathbf{t}$ can be computed as the cumulative sum of $\mathrm{d}\mathbf{t}$. Now, we can interpolate the east wind $\mathbf{W}_x(t)$ and north wind $\mathbf{W}_y(t)$ at $(\mathbf{x}, \mathbf{y}, \mathbf{t})$, by trilinear interpolation. Fig. 3 depicts the eight grid points used for interpolating the value on the target location. The function value is C_1 continuous (blue region) everywhere except on the grid points and the edges where it is C_0 continuous (orange region). As a numerical method, this continuity condition is adequate for the gradient-based optimizer to perform finite-difference by sampling from interior points (blue region). Having computed $\mathbf{W}_x(t)$ and $\mathbf{W}_y(t)$, we can compute the $\mathbf{W}_t$ and $\mathbf{W}_c$ along $\mathbf{T}$ by

$$\begin{aligned} \mathbf{W}_t &= \ \ \mathbf{W}_x \sin\boldsymbol{\theta} + \mathbf{W}_y \cos\boldsymbol{\theta} \\ \mathbf{W}_c &= -\mathbf{W}_x \cos\boldsymbol{\theta} + \mathbf{W}_y \sin\boldsymbol{\theta}, \end{aligned} \tag{5}$$

where

$$\boldsymbol{\theta} = \tan^{-1} \frac{\sin(\mathbf{x}_2 - \mathbf{x}_2)\cos\mathbf{y}_2}{\cos\mathbf{y}_1 \sin\mathbf{y}_2 - \sin\mathbf{y}_1 \cos\mathbf{y}_2 \cos(\mathbf{x}_2 - \mathbf{x}_1)} \tag{6}$$

is the navigational bearing angle. Now, we notice that the $\mathbf{t}$ obtained from this newly interpolated wind is inconsistent with the initial guess. To ensure consistency, Algorithm 1 iteratively updates the values of $\mathrm{d}\mathbf{t}$, its cumulative sum $\mathbf{t}$, and wind velocity at $\mathbf{t}$ until they converge. These quantities are updated in a vectorized way instead of solving one time step at a time sequentially. The convergence is checked by evaluating the residual $\mathcal{R}(\mathbf{t})$ between the previous and updated time steps using the residual function; the convergence is achieved when the residual value falls below a predefined threshold ϵ. Finally, the total travel time t_f is calculated by summing the time intervals $\mathrm{d}\mathbf{T}$.

Algorithm 1 Travel Time Computation with Variable Wind

Input:

- Trajectory $\mathbf{T}$
- True airspeed V_{TAS}
- Wind data $\mathbf{W}(t)$
- Integration fineness N

Output:

Travel time t_f

Generate $\mathbf{T}$ based on $\mathbf{x}$ and $\mathbf{y}$;
Calculate GC distance $\mathrm{d}\mathbf{x}$ between N integration points (Eq. (3));
Estimate travel time $\mathrm{d}\mathbf{t}$ (Eq. (4));
Calculate bearing θ along $\mathbf{T}$ (Eq. (6));
Interpolate and calculate $\mathbf{W}_t(\mathbf{t})$ and $\mathbf{W}_c(\mathbf{t})$ at an initial guess $\mathbf{t}$ (Eq. (5));
Estimate time stamp $t_j = \sum_{i=1}^{j} \mathrm{d}t_i$, denoted as $\mathbf{t}$;
Set count $k = 0$;
while $\mathbf{R}(\mathbf{t}) \geq \varepsilon$ **do**
    Interpolate $\mathbf{W}_t^k(\mathbf{t})$ and $\mathbf{W}_c^k(\mathbf{t})$ based on $\mathbf{t}^k$ (Eq. (5));
    Estimate $\mathrm{d}\mathbf{t}^{k+1}$ based on $\mathrm{d}\mathbf{x}^k$, V_{TAS}, $\mathbf{W}_t^k(\mathbf{t})$, and $\mathbf{W}_c^k(\mathbf{t})$ (Eq. (4));
    Estimate $\mathbf{t}^{k+1} = \sum_{i=1}^{j} \mathrm{d}\mathbf{t}^{k+1}$;
    $\mathbf{R}(\mathbf{t}) = ||\mathbf{t}^{k+1} - \mathbf{t}^k||_2$ (L_2-norm);
    $k \leftarrow k + 1$
end while
$t_f = \sum \mathrm{d}\mathbf{t}$.

D. Optimization Algorithm

To find the optimum trajectory (as defined by the control point coordinates), we use a gradient-based nonlinear programming algorithm, which is known to be more efficient than the gradient-free counterparts. As the problem is box-constrained (i.e., only lower and upper bound of design variables are present as constraints), we use a quasi-Newton algorithm, namely the Broyden [18]–Fletcher [19]–Goldfarb [20]–Shanno [21] (BFGS) algorithm. As a second-order algorithm, the Jacobian and Hessian of the function are needed. The Jacobian is obtained by performing finite-difference on the design variable, while the Hessian is calculated using a dense quasi-Newton approximation. The update rule of the approximated Hessian $\mathbf{B}$ is

$$\mathbf{B}^+ = \mathbf{B} + \frac{(\mathbf{y} - \mathbf{B}\mathbf{s})(\mathbf{y} - \mathbf{B}\mathbf{s})^\top}{(\mathbf{y} - \mathbf{B}\mathbf{s})^\top \mathbf{s}}, \tag{7}$$

where $\mathbf{y} = \nabla f(\mathbf{x}^+) - \nabla f(\mathbf{x})$ is the change in Jacobian, $\mathbf{s} = \mathbf{x}^+ - \mathbf{x}$ is the update step, and the superscript $^+$ refers to the next iteration. However, it is preferable to directly update the inverse of the approximated Hessian $\mathbf{H} = \mathbf{B}^{-1}$, instead of updating $\mathbf{B}$ first and calculating its inverse. By applying

Sherman-Morrison-Woodbury formula on Eq. (7), the update rule of $\mathbf{H}$ is

$$\mathbf{H}^{+} = \mathbf{H} + \frac{(\mathbf{s} - \mathbf{H}\mathbf{y})(\mathbf{s} - \mathbf{H}\mathbf{y})^{\top}}{(\mathbf{s} - \mathbf{H}\mathbf{y})^{\top}\mathbf{y}}. \tag{8}$$

Having obtained Eq. (8), the descent direction can then be calculated as

$$\mathbf{d} = -\mathbf{H}\nabla f(\mathbf{x}), \tag{9}$$

and a line search is applied along $\mathbf{d}$ to get the maximum descent in the function value. Assuming the line search returned an optimal step length of α, the design variable will be updated by

$$\mathbf{x}^{+} = \mathbf{x} + \alpha\mathbf{d}. \tag{10}$$

III. Results

We apply the developed methodology to several popular flights destinations from the Hong Kong International Airport (HKG), including London Heathrow Airport (LHR), Seoul Incheon International Airport (ICN), and Taipei Taoyuan International Airport (TPE). These flight sectors represent long-, medium-, and short-haul flights, respectively. Trajectories for these flights are optimized under a wide range of date and time to capture the seasonality and variation of how weather conditions affect travel time.

A. Case Study of Single Trajectory

We use 19 design points to optimize the trajectory between HKG and LHR on the day of 12 Jan 2022. Along the trajectory, 1,000 integration points are used to evaluate the travel time, with an average time step of $35.2\,\mathrm{s}$ for LHR–HKG and 40.8 for HKG–LHR.

Sector	OPT	GC	QAR
LHR–HKG	9h 46.8m	9h 28.2m	10h 49.2m
HKG–LHR	11h 51.6m	11h 18.6m	13h 9.0m

TABLE I. Travel time (in hours and minutes) for the optimized (OPT), great circle (GC), and quick access record (QAR) trajectory.

Travel time for the optimized (OPT), great circle (GC), and quick access recorder (QAR) trajectory (from our airline partner) of LHR–HKG (mostly tailwind) and HKG–LHR (mostly headwind) are tabulated in Table I. For a fair comparison, travel time of QAR is re-calculated using the same method as in our optimization procedure, instead of the raw QAR data. The optimal travel time is several minutes faster than the GC trajectory, and much less than that of the QAR trajectory. These three trajectories of LHR–HKG and HKG–LHR are plotted in Figs. 5a and 5b, respectively, for a visual comparison. Note that in reality, there might be several factors that hinder aircraft from flying their most fuel efficient routes. For example, the aircraft might want to avoid the Maastricht Upper Area Control Centre (MUAC) area, which is considered one of the busiest and most complex airspace. Also, only part of the airspace in China is open of civil aviation, so aircraft are required to strictly follow certain waypoints and paths, where further unconstrained optimization might not be possible. However, as mentioned in Section I, we would like to explore the largest potential in time saving by optimizing the cruise trajectory, as the air traffic management regulations keep evolving with the advancement of technology.

To visually demonstrate the effectiveness of our algorithm, Fig. 6 overlays the trajectory presented in Fig. 5b on the time-dependent wind field. The trajectory and wind field is plotted from $T = 0$ to $T = t_f$ at nine equally distributed time stamps. The great circle is plotted in red, the optimized the trajectory is plotted in black, while the blue star marks the destination (LHR). The background shows wind field, where green and red color indicate the favorability of the location, while black arrows show the local wind magnitude and direction at T. Areas with tailwind (favourable) is shown in green, while that with headwind (unfavourable) is shown in red. The idea of favorability is inspired by the velocity superposition principle explained in Fig. 4. Conceptually, favorability is the additional velocity that an aircraft can gain (or lose) from the tailwind (or headwind), which can be calculated by using Eq. (4). White area means the wind does not change aircraft ground speed (but may still cause its heading to be misaligned with the trajectory). We observe that the optimized trajectory avoids strong headwind experienced by the GC when $T \leq 7.48\,\mathrm{h}$, and leads to a zone of strong tailwind afterward.

B. Statistical Study of Airline Operations

Having demonstrated the effectiveness of the developed algorithm, we further investigate its benefits to airline by evaluating the travel time reductions on actual trajectories, using the three flight sectors mentioned above. In particular, we use representative flights operated by CX to the above-mentioned three destinations within the period of 1 January 2020 to 31 December 2020, including 621 HKG–TPE flights, 172 HKG–ICN flights, and 527 HKG–LHR flights. These 1,320 flight trajectories are optimized using the newly developed algorithm based on information obtained from QAR data, including the date and time of the flight, the starting and ending position of the cruise segment, and the average true airspeed. The optimized travel time is then compared against the one calculated by the corresponding trajectory recorded in QAR; the distribution of the travel time reduction is shown in Fig. 7 for the three flight sectors. Not surprisingly, the travel time reduction (in hours) is shown to be proportional to the total travel time, where more substantial travel time reduction is observed on long-haul flights. Taking the average value of the relative time reduction (in percentage), our algorithm reduces 10%, 14%, and 6% of the travel time for HKG-TPE, HKG-ICN, and HKG-LHR sector, respectively. We observe that for HKG-TPE flights, the very short cruising range limits the room for improvement. On the other hand, the baseline travel time for HKG-LHR is relatively long, so the resultant percentage time reduction is less substantial. These observations might explain why the gains achieved in these two sectors are relatively lower than that of HKG-TPE. In airline operations, where both financial and environmental considerations are

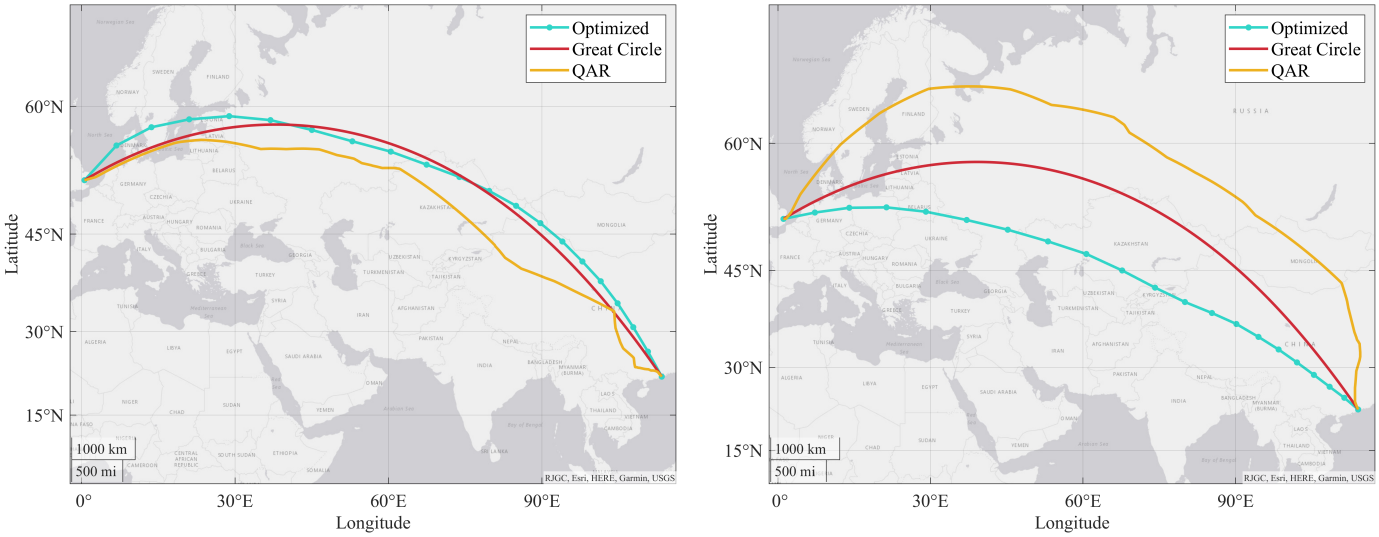

(a) Optimal t_f from LHR to HKG is 9 hours 46.8 minutes.

(b) Optimal t_f from HKG to LHR is 11 hours and 18.8 minutes.

Figure 5. Comparison of the optimized trajectory and the GC trajectory between HKG and LHR on 12 Jan 2022.

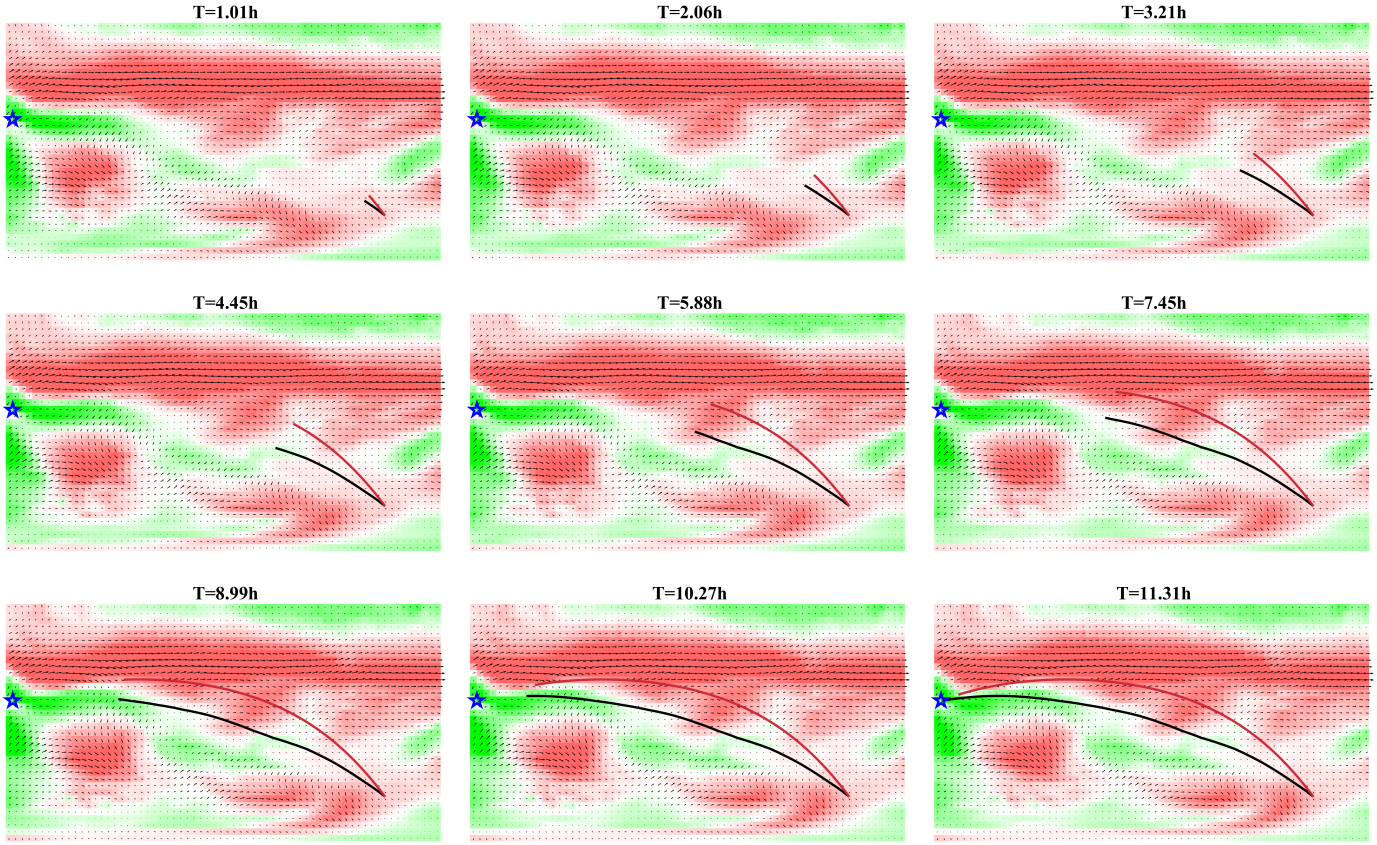

Figure 6. Trajectory from $T = 0$ to $T = t_f$ at nine equally distributed time stamps. The background color indicates the favorability of the location, with green and red corresponding to favorable (with tailwind) and unfavorable (with headwind) condition, respectively. Within the wind field, the black arrows show the local wind magnitude and direction at T.

vitally important, this outcome can contribute to a substantial reduction in operating cost and operational block time, thereby increasing overall efficiency and customer satisfaction.

IV. Conclusion

In summary, this research paper presented a new method to solve for the time-minimal aircraft trajectory problem in the presence of unsteady wind conditions. The proposed approach

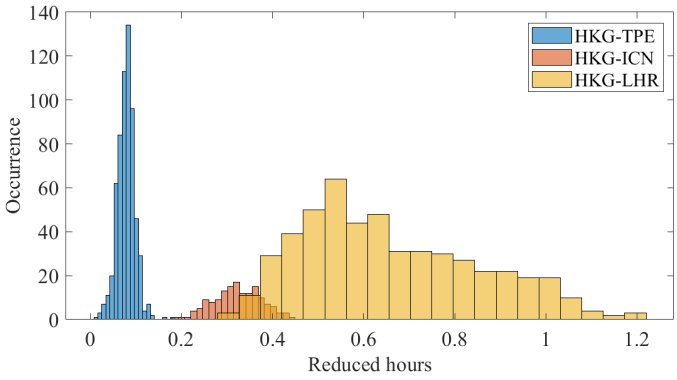

Figure 7. Histogram of reduced travel time between HKG–TPE, HKG–ICN, and HKG–LHR.

formulates the problem as a shape optimization task to enhance flexibility in flight planning compared to traditional grid-based algorithms. This algorithm works on a continuous domain, which reduces error and computational cost associated with spatial discretization. By accurately considering the dynamic, time-dependent wind conditions, the optimized trajectories achieve a balance between minimizing distance and avoiding headwinds, as shown in the case study involving flights between HKG and LHR. We further demonstrated the effectiveness of our approach on 1,320 flights that represent long-, medium-, and short-haul sectors, which consistently showed notable travel time reduction. To conclude, this research can bring practical benefits to the airline industry with its potential to enhance operational efficiency, reduce fuel consumption, and mitigate environmental impact. Future work will focus on incorporating considerations such as no-fly zones and mountainous areas for more realistic trajectory optimizations, as well as exploring a two-stage optimizer that combines a grid-based pre-optimization and grid-free methods to assure global optimality.

Acknowledgment

The authors would like to extend their sincere appreciation to the University Grant Council of the Hong Kong Special Administration Region for its financial support to the first and second authors through the Hong Kong PhD Fellowship Scheme (HKPFS). In addition, the authors acknowledge Cathay Pacific Airways Limited for providing the data used in this study under the Data Partnership Agreement between the airline and the Department of Mechanical and Aerospace Engineering, HKUST.

References

[1] International Air Transport Association (IATA), *Economic Performance of the Airline Industry - 2020 Edition*, 2020. [Online]. Available: https://www.iata.org/en/iata-repository/publications/economic-reports/airline-industry-economic-performance---october-2021---report/

[2] International Civil Aviation Organization, "2019 environmental report," 2019. [Online]. Available: https://www.icao.int/environmental-protection/pages/envrep2019.aspx

[3] P. Belobaba, A. Odoni, and C. Barnhart, *The Global Airline Industry*, 2nd ed. John Wiley & Sons, 2015.

[4] B. Sridhar, H. K. Ng, and N. Y. Chen, "Aircraft trajectory optimization and contrails avoidance in the presence of winds," *Journal of Guidance, Control, and Dynamics*, vol. 34, no. 5, pp. 1577–1584, 2011.

[5] C. Petres, Y. Pailhas, P. Patron, Y. Petillot, J. Evans, and D. Lane, "Path planning for autonomous underwater vehicles," *IEEE transactions on robotics*, vol. 23, no. 2, pp. 331–341, 2007.

[6] Y.-C. Chang, R.-S. Tseng, G.-Y. Chen, P. C. Chu, and Y.-T. Shen, "Ship routing utilizing strong ocean currents," *The Journal of Navigation*, vol. 66, no. 6, pp. 825–835, 2013.

[7] E. W. Dijkstra, "A note on two problems in connexion with graphs," *Numerische mathematik*, vol. 1, no. 1, pp. 269–271, 1959.

[8] P. E. Hart, N. J. Nilsson, and B. Raphael, "A formal basis for the heuristic determination of minimum cost paths," *IEEE transactions on Systems Science and Cybernetics*, vol. 4, no. 2, pp. 100–107, 1968.

[9] A. Stentz, "Optimal and efficient path planning for partially-known environments," in *Proceedings of the 1994 IEEE international conference on robotics and automation*. IEEE, 1994, pp. 3310–3317.

[10] H. Wang, W. Mao, and L. Eriksson, "A three-dimensional dijkstra's algorithm for multi-objective ship voyage optimization," *Ocean Engineering*, vol. 186, p. 106131, 2019.

[11] D. Delahaye, S. Puechmorel, P. Tsiotras, and E. Féron, "Mathematical models for aircraft trajectory design: A survey," in *Air Traffic Management and Systems: Selected Papers of the 3rd ENRI International Workshop on ATM/CNS (EIWAC2013)*. Springer, 2014, pp. 205–247.

[12] T. Lolla, M. P. Ueckermann, K. Yiğit, P. J. Haley, and P. F. Lermusiaux, "Path planning in time dependent flow fields using level set methods," in *2012 IEEE International Conference on Robotics and Automation*. IEEE, 2012, pp. 166–173.

[13] B. Girardet, L. Lapasset, D. Delahaye, and C. Rabut, "Wind-optimal path planning: Application to aircraft trajectories," in *2014 13th International Conference on Control Automation Robotics & Vision (ICARCV)*. IEEE, 2014, pp. 1403–1408.

[14] D. A. Masters, N. J. Taylor, T. Rendall, C. B. Allen, and D. J. Poole, "Review of aerofoil parameterisation methods for aerodynamic shape optimisation," in *53rd AIAA Aerospace Sciences Meeting*, 2015.

[15] R. M. Hicks and P. A. Henne, "Wing design by numerical optimization," *Journal of Aircraft*, vol. 15, no. 7, pp. 407–412, 1978.

[16] T. Lassila and G. Rozza, "Parametric free-form shape design with pde models and reduced basis method," *Computer Methods in Applied Mechanics and Engineering*, vol. 199, no. 23, pp. 1583–1592, 2010.

[17] T. W. Sederberg and S. R. Parry, "Free-form deformation of solid geometric models," in *Proceedings of the 13th annual conference on Computer graphics and interactive techniques*, 1986, pp. 151–160.

[18] C. G. Broyden, "The convergence of a class of double-rank minimization algorithms 1. general considerations," *IMA Journal of Applied Mathematics*, vol. 6, no. 1, pp. 76–90, 1970.

[19] R. Fletcher, "A new approach to variable metric algorithms," *The computer journal*, vol. 13, no. 3, pp. 317–322, 1970.

[20] D. Goldfarb, "A family of variable-metric methods derived by variational means," *Mathematics of Computation*, vol. 24, no. 109, pp. 23–26, 1970.

[21] D. F. Shanno, "Conditioning of quasi-newton methods for function minimization," *Mathematics of computation*, vol. 24, no. 111, pp. 647–656, 1970.